International Journal of Biological Macromolecules 220 (2022) 1277–1286

Contents lists available at ScienceDirect

International Journal of Biological Macromolecules

journal homepage: www.elsevier.com/locate/ijbiomac

Formation of biocompatible MgO/cellulose grafted hydrogel for efficient bactericidal and controlled release of doxorubicin

Iram Shahzadi [a], Muhammad Islam [a,*], Hamid Saeed [a], Ali Haider [b], Anum Shahzadi [c], Junaid Haider [d], Nadeem Ahmed [e], Anwar Ul-Hamid [f], Walid Nabgan [g,*], Muhammad Ikram [h,*], Hassaan Anwer Rathore [i]

[a] Punjab University College of Pharmacy, Allama Iqbal Campus, University of the Punjab, Lahore 54000, Punjab, Pakistan
[b] Department of Clinical Sciences, Faculty of Veterinary and Animal Sciences, Muhammad Nawaz Shareef University of Agriculture, Multan 66000, Punjab, Pakistan
[c] Faculty of Pharmacy, The University of Lahore, Lahore 54000, Pakistan
[d] Tianjin Institute of Industrial Biotechnology, Chinese Academy of Sciences, Tianjin 300308, PR China
[e] Centre of Excellence in Molecular Biology, University of the Punjab, Lahore, Punjab, Pakistan
[f] Core Research Facilities, King Fahd University of Petroleum & Minerals, Dhahran 31261, Saudi Arabia
[g] Departament d'Enginyeria Química, Universitat Rovira i Virgili, Av Països Catalans 26, 43007 Tarragona, Spain
[h] Solar Cell Applications Research Lab, Department of Physics, Government College University Lahore, Lahore 54000, Punjab, Pakistan
[i] College of Pharmacy, Qatar University, Doha 2713, Qatar

ARTICLE INFO

Keywords:
Cellulose nanocrystals (CNC)
Poly (acrylic acid) (PAA)
Hydrogel

ABSTRACT

In this study, MgO-doped CNC-g-PAA hydrogel was synthesized by grafting poly (acrylic acid) (PAA) onto cellulose nanocrystals (CNC) and then doped Magnesium oxide (MgO) using pH 7.0 and 12.0 to obtain an efficient nanocomposite hydrogel for antibacterial and anti-cancer activities. The synthesized nanocomposite hydrogels were evaluated by detailed characterization and confirmed the formation of a well-interconnected porous structure. MgO/CNC-g-PAA (pH = 12.0) exhibited improved bactericidal tendencies towards gram-negative and gram-positive bacteria, which was further investigated by *in-silico* molecular docking analyses and also examined the reactive oxygen species production by photocatalysis and free radical-scavenging assay. After this, Doxorubicin (DOX), a model anticancer drug, was successfully loaded into nanocomposites (~79 %) by electrostatic interaction and confirmed pH-triggered based release, which was over 53.7 % in 24 h. Finally, *in vitro* cytotoxicity-based analysis confirmed the improved antitumor efficacy of nanocomposite hydrogels. These findings revealed that MgO/CNC-g-PAA hydrogels might be prospective carriers for controlled drug delivery.

1. Introduction

Cancer, the world's second most significant cause of mortality [1], encompasses a variety of illnesses that emerge as a consequence of uncontrolled proliferation of malignant cells and can infiltrate or spread to other body areas [2]. Conventional cancer drug delivery is hampered by non-specific dispersion in biological systems, poor target selection, low bioavailability [3], pervasive toxicity, and most critically, the development of multiple drug resistance (MDR) [2,4–6]. In recent years, researchers frequently used nanotechnology to overcome these barriers [7], which is considered an emerging frontier in developing multifunctional and robust nanomaterials, such as nanoparticle-filled polymer composites (< 100 nm) [8–10], hydrogels, nanosphere and microsphere, micelles, and liposome for targeted drug delivery [11]. Hydrogels are chemically or physically cross-linked networks that can absorb a substantial quantity of liquid such as water or biological fluid without dissolving [12–14]. Thus, high swelling property of hydrogels permits them to retain an enormous volume of liquid and soft consistency [15,16], additionally, high porosity enables efficient drug loading and subsequent drug-releasing at a determined rate through gel matrix [17,18].

Among natural polymers, cellulose, composed of glucose-based repeating β-1,4-glycosidic bonds, is most appealing because of its unique qualities, including its biodegradability, nontoxicity, abundance on the planet, and presence of hydroxyl groups (OH) on its backbone, which enables chemical modification using variety of functional

* Corresponding authors.
E-mail addresses: islam.pharmacy@pu.edu.pk (M. Islam), walid.nabgan@urv.cat (W. Nabgan), dr.muhammadikram@gcu.edu.pk (M. Ikram).

https://doi.org/10.1016/j.ijbiomac.2022.08.142
Received 19 June 2022; Received in revised form 12 August 2022; Accepted 17 August 2022
Available online 27 August 2022

components [19]. Strong acid hydrolysis of this linear polymer significantly affects surface chemistry along with the reduction of its size to a nano-level and finally, shifted to a rod-shaped structure, known as cellulose nanocrystals (CNCs) [20,21]. Nevertheless, various studies revealed that natural polymers-based hydrogels like alginate, chitosan, or CNCs have weak mechanical properties [22], destabilizing drug delivery process, resulting in simultaneous release of a drug. The fusion of CNC with synthetic biopolymer may help cover this research gap and provide opportunities to obtain desired mechanical properties. Polyacrylic acid (PAA), a typical hydrophilic and pH-sensitive biopolymer, contains pendant carboxylic acid groups adequate for interacting with hydroxyl groups on the CNC surfaces [23]. CNCs are mostly insoluble fibres because of their partially to fully crystalline structure, while incorporating CNC into PAA significantly reduced fiber diameter and allowed it to well disperse in PAA matrix [24]. So, the copolymerized hydrogel exhibits a great variety of unique and novel properties, including considerable swelling capacity with improved mechanical and stimuli-responsive properties, which allow them to become efficient for drug administration and other biological applications [25].

Parallel to hydrogel advancements, various research groups have successfully integrated several kinds of inorganic nanoparticles with hydrogel to develop a hydrogel-based hybrid system and obtain specific functional and mechanical properties [26,27]. The incorporation of nanoparticles into a hydrogel matrix is regarded to provide structural diversity and a variety of properties enhancements as well as reduce risk factors associated with human health and the environment [28,29]. Among the several inorganic metal oxides, magnesium oxide (MgO) nanoparticles (NPs) are well-known for their biological potential as an antibacterial, anti-oxidant, and anticancer agent, with added benefit of being nontoxic and very simple to produce [30]. Additionally, the US Food and Drug Administration recognizes MgO as safe material (21CFR184.1431) [31–33]. Like other metal ions, MgO nanomaterials have also been attributed to generating reactive oxygen species (ROS) (Leung et al., 2014). Photogenerated ROS considered as efficient antimicrobial and anticancer agents, can damage cell membrane by lipid peroxidation resulting in cell death because of the loss of respiratory activity [34–37]. In addition, free radicals also can remove organic pollutants (dye degradation) from polluted water, which has become a worldwide concern owing to pesticides, industrial waste, and waterborne pathogens, such as *Staphylococcus aureus* (Gram-positive) and *Escherichia coli* (*E. coli*) (Gram-negative) bacteria. Several studies revealed that varying concentrations of Mg-doped with either CNC, graphene oxide (GO), or ZnO nanorods result in enhanced photocatalytic and bactericidal properties [38–40]. Numerous nanocomposites have been used to deliver cancer vaccines and adjuvants [41], which respond specifically to the tumour microenvironment, resulting in increased drug accumulation at the tumour site, decreased side effects on non-cancerous tissues, and enhanced therapeutic effect, such as the modified MoS2-nanocomposite [42]. Similarly, magnesium may operate as a preventive agent in colorectal carcinogenesis [43], and *co*-assembly of DOX and nanomedicines can form temperature-sensitive polymers for targeted treatment of liver cancer [44]. However, a drug-loaded copolymerized hydrogel (CNC-g-PAA)-based hybrid system with doped MgO nanoparticles has not been elucidated for evaluating the multifunctional properties including targeted drug delivery.

In this study, we grafted vinyl monomers such as PAA (-COOH) onto surface of CNCs to enhance its absorption capacity and then doped CNC-g-PAA with MgO, which binds to carboxyl groups, to improve its mechanical property for efficient drug delivery system. The synthesized material was evaluated by detailed characterization of morphological, optical, structural, functional, and chemical composition analyses. In addition, molecular docking-based analyses performed to investigate mechanism behind bacterial strains inhibition through synthesized MgO/CNC-g-PAA. Then, drug delivery potential of metal-doped copolymerized hybrid system was evaluated with effect of pH. Doxorubicin (DOX) used as standard drug against cancer therapy which bound efficiently with MgO/CNC-g-PAA and confirmed *in vitro* cytotoxicity and release rate of bound DOX from nanocomposite. This system significantly improves drug loading and releasing efficacy for cancer therapy which could be a great promise for further improvement of targeted drug delivery by copolymerized hydrogel-based hydride system.

2. Materials and methods

2.1. Synthesis of cellulose nanocrystals (CNC)

CNC was prepared *via* H_2SO_4 hydrolysis of Avicel using a reported protocol [45,46]. Briefly, 10 g Avicel was hydrolyzed for 30 min at 45 °C in 64 % (*w*/w) H_2SO_4 solution with a total volume of 100 mL. The reaction was terminated through the addition of 1900 mL cooled deionized (DI) water to a yellow-brown mixture and allowed to settle down the suspended particles overnight at ambient temperature (25 °C–28 °C). The surplus water was decanted and remaining sediment was collected by centrifugation (3100 *g*, 15 min), washed 3–4 times with water until suspension became clear, and then neutralized by 0.25 M NaOH. Finally, the leftover suspension was sonicated using Vibracell Sonicator for 15 min and determined the total solid content by drying at 105 °C to attain a constant weight. The stock of synthesized CNC was prepared to 97.5 mg/mL and stored at 4 °C for further experiments.

2.2. Synthesis of hydrogel (CNC-g-PAA)

CNC-g-PAA was prepared using a slightly modified version of the reported method described by [23]. Fig. 1a illustrates the synthesis procedure of CNC-g-PAA. Briefly, ~5 mL of synthesized CNC was introduced to 75 mL DI water. The final CNC concentration in mixture was ~6 mg/mL, which was sonicated for 40 min and degassed under vacuum. Then, 5 mL of sodium persulfate solution (13 mg/mL) poured into reaction container and mixture was stirred at 50–55 °C for 25 min. Subsequently, PAA was introduced, with a weight ratio of CNC to PAA (1:6), dropwise to the reaction mixture within 1 h under incubation at 60–65 °C. After addition, the mixture was further incubated for another hour. Then the mixture was cooled at ambient temperature and centrifuged at 3100 *g* for 15 min to harvest the synthesized CNC-g-PAA, which was highly stable and not precipitated by centrifugation. The synthesized hydrogel was redispersed in DI water two times to eliminate the impurities and unbound polymer [47] then lyophilized the sample prior to storage.

2.3. Synthesis of hybrid hydrogel (MgO/CNC-g-PAA)

MgO/CNC-g-PAA nanocomposite hydrogel was synthesized using a slightly modified method version [48,49], illustrated in Fig. 1b. Briefly, 200 mg of synthesized powder of CNC-g-PAA was dispersed in 5 mL ddH_2O and final concentration was 40 mg/mL. Then, 25 mL of 100 mM $MgCl_2{\cdot}6H_2O$ was added to dispersed CNC-g-PAA under heating at 80–85 °C with continuous stirring, adjusted the pH (7.0 and 12.0) of the hydrogel mixture using aqueous NaOH (0.5 M) solution and incubated for 30 min. Subsequently, the synthesized MgO/CNC-g-PAA was harvested using centrifugation (3100 *g*, 15 min) and redispersed in DI water three times to remove residual. Samples were dried at 105 °C and obtained a fine powder.

All other materials and methods are described in detail in the supporting information, experimental section.

3. Results and discussion

3.1. Characterization of synthesized nanocomposite hydrogels

MgO/CNC-g-PAA was fabricated by graft polymerization of PAA on CNC, and doped with MgO by co-precipitation method (Fig. 1). The fabricated nanocomposite hydrogel was evaluated with detailed

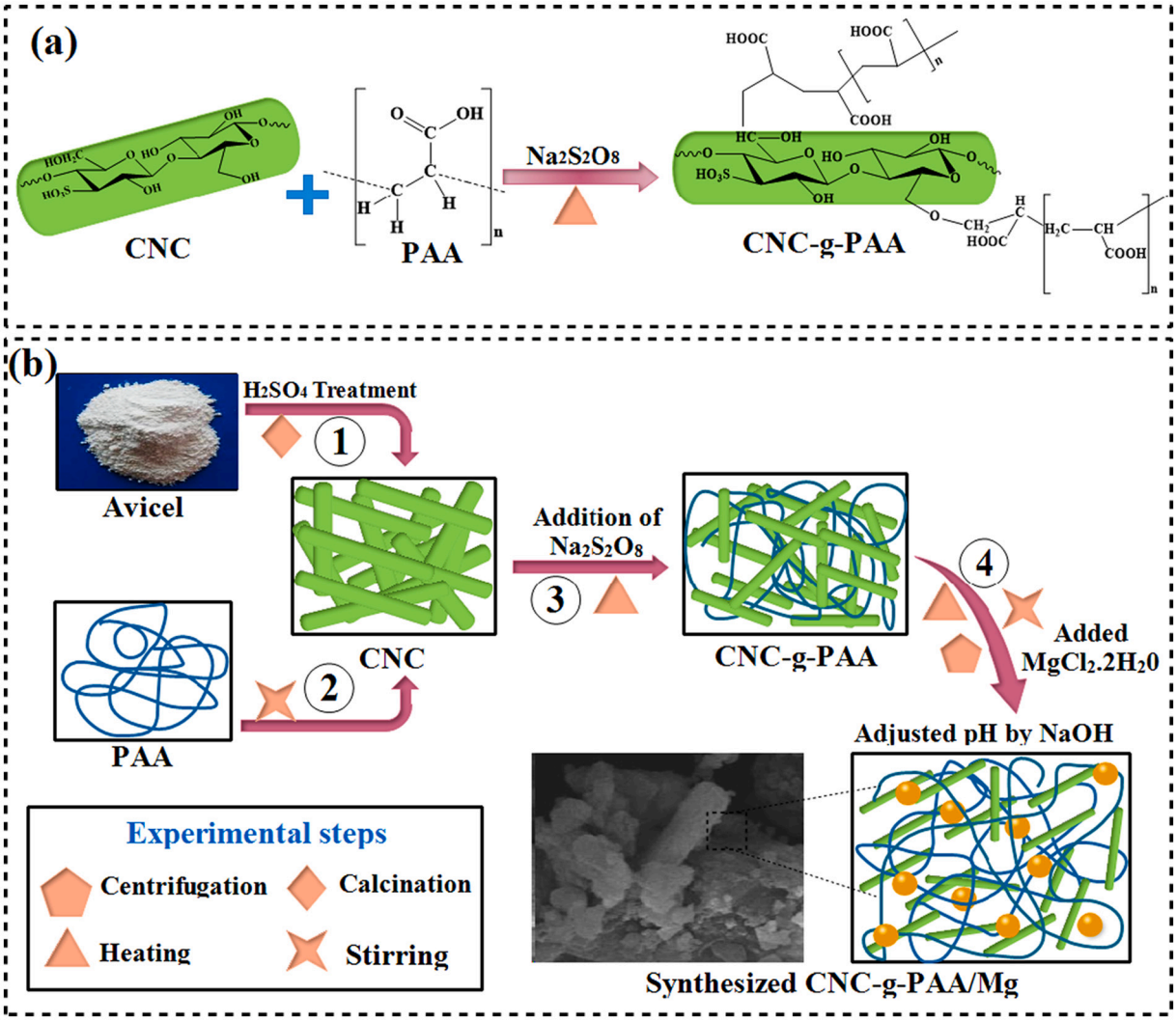

Fig. 1. Schematic illustration of synthesized MgO/CNC-g-PAA. Panel (a) shows the chemical interaction between CNC and PAA in the presence of $Na_2S_2O_8$. Panel (b) illustrates the synthesis of MgO/CNC-g-PAA.

characterizations as FTIR, XRD, SAED, UV–vis spectroscopy, HR-TEM, EDS, and DSC. These results demonstrated successful doping of MgO on CNC-g-PAA, with improved bactericidal potential and drug loading or release efficiency of nanocomposite hydrogel against cancer treatment.

The chemical constituents and functional characterization of synthesized nanocomposite hydrogels were evaluated through FTIR analysis (Fig. 2a). CNC presented characteristic peaks at 3000–3600 cm^{-1} (O—H stretching), 1050 cm^{-1} (C–O–C vibrations) [50], and >C=O stretching at 1645 cm^{-1} [51]. Moreover, PAA characteristic bands at 2951 cm^{-1} indicate (-CH- stretching vibrations), 1711–1721 cm^{-1} (C═O stretching), as well as peak after oxidation of carboxylic group at 1570–1600 cm^{-1} (C=O) [23,52–54]. CNC-g-PAA exhibited similar FTIR spectra comprising OH, COC, and C═O (COOH) peaks of CNC and PAA, indicating the effective graft polymerization of PAA onto CNC backbone linkages. Highs at 1418 cm^{-1} are attributed towards symmetrical and asymmetrical stretching vibrations of carboxylate (OC=O) [55], whereas absorption band of cubic MgO found at 854 cm^{-1} [56]. The FTIR spectra of MgO/CNC-g-PAA display all the predicted peaks, including -COOH (or -COONa), -OH, and -MgO; however, the intensity of MgO peak enhanced significantly at pH = 12.0 (around 854 cm^{-1}), suggesting enhanced binding between COOH (acrylic acid) and MgO throughout reaction. This result validated successful substitution of MgO in CNC-g-PAA as shown by shift in signal intensity.

X-ray diffraction in 2θ range of 10°-70° was employed to investigate the structural characteristics and phase composition of CNC, CNC-g-PAA, and MgO/CNC-g-PAA at pH = ~7.0 and 12.0, as shown in Fig. 2b. The major characteristic crystalline peaks in CNC sample were found at 2θ of 12°, 19.5°, 22.4°, and 33.9° [57,58]. CNC possesses crystalline structure because cellulose Avicel was depolymerized more successfully in amorphous zone than crystalline region, which retained intact after acid hydrolysis [59,60]. After grafting polymerization of PAA with backbone CNC chains, almost all peaks were seen in XRD patterns of CNC-g-PAA, however, signal strength was drastically decreased due to an amorphous structure of PAA [59]. This result depicted CNC successful incorporation *via* graft polymerization [61]. In diffraction spectra of MgO-loaded CNC-g-PAA at pH 7.0 and 12.0, the characteristic heights at 38.4° (222), 44.37° (400), 59.17° (511), 64.52° (440) confirmed existence of doped MgO in CNC-g-PAA corroborated cubic structure of MgO as indicated by (JCPDS File 00-030-0794) [62].

Following this the optical characteristics (Fig. S3) and thermal stability (Fig. S4) of synthesized materials were validated through UV–Vis spectroscopy and DSC, separately, and were explained including SAED analysis in supporting information, supporting text.

3.2. Size, shape, and morphology of nanocomposite hydrogels

The surface topography of pure (CNC), grafted (CNC-g-PAA), and

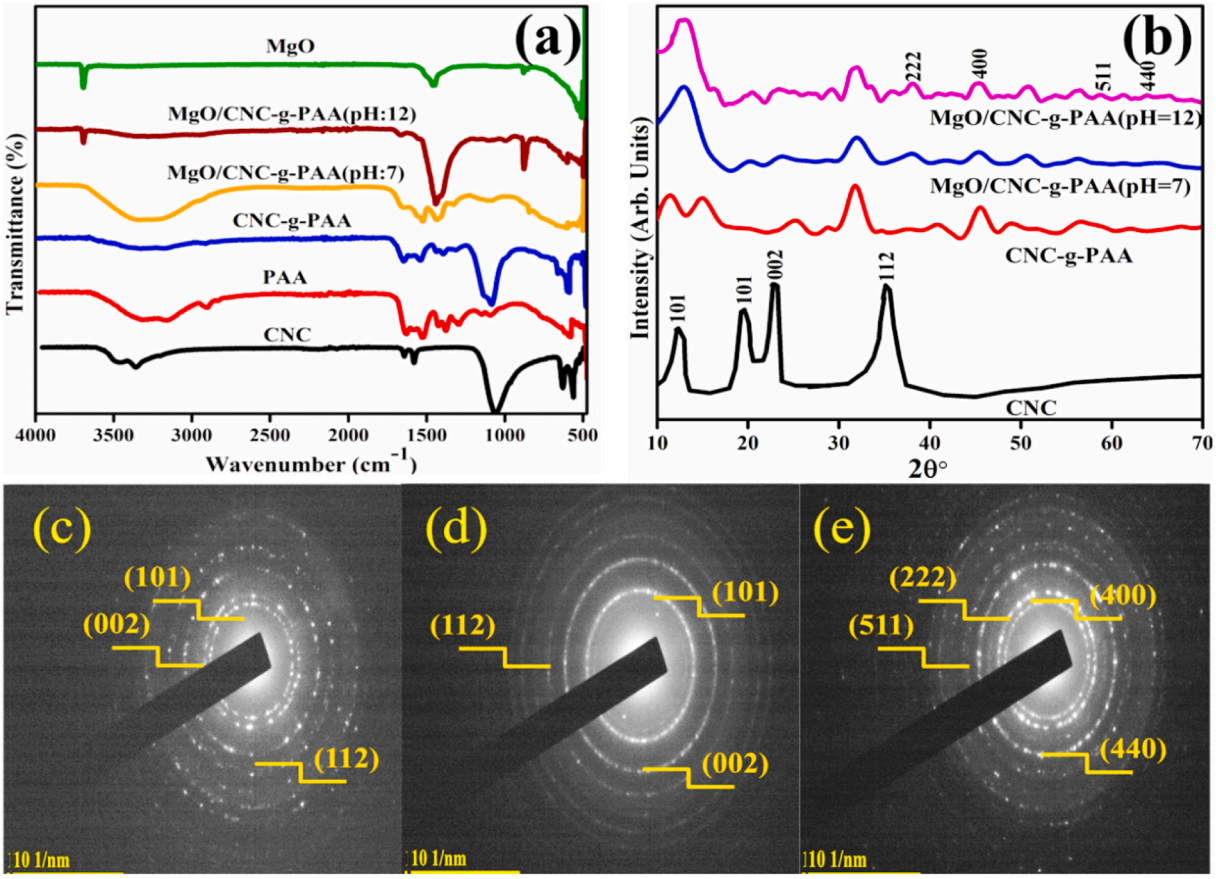

Fig. 2. (a) FTIR spectra, (b) XRD pattern, (c-e) SAED pattern of CNC, CNC-g-PAA, and MgO/CNC-g-PAA nanocomposites

doped (MgO/CNC-g-PAA at pH = 12.0) composites were observed by HR-TEM (Fig. 3). TEM images clearly revealed rod-shape of CNC, and CNC-g-PAA as highly porous materials. Agglomeration could be seen in MgO/CNC-g-PAA (Fig. 3c), which occurred due to particles strong interactions at nanoscale in existence of MgO [63]. Subsequently, as shown in Fig. 3(d-f), highly magnified TEM images (10 nm) were used to compute interlayer d-spacing of synthesized samples by displaying lattice fringes for crystallographic planes. The calculated d-spacing for CNC, CNC-g-PAA, and MgO/CNC-g-PAA measured as ~0.284, 0.288, and 0.207 nm, correspondingly, and satisfy theoretical d-spacing of (400) MgO planes (JCPDS File 00–030-0794).

EDS used to ascertain the constituent components of pure, grafted, and doped samples (Fig. 3). The existence of Mg and O peaks verified production of MgO, which is well incorporated with CNC-g-PAA nanocomposite. While, O and C signal peaks show successful integration of PAA and CNC into the lattice. Moreover, Na peak could ascribe from NaOH solution added during nanocomposite hydrogel fabrication process. The appearance of extra elements (Au, Cl) could be attributed to detector's coating material and high background count elements.

3.3. Anti-microbial and in silico analysis

The *in-vitro* bactericidal efficiency of CNC, CNC-g-PAA, and MgO/CNC-g-PAA (pH 7.0 and 12.0) was evaluated by measuring inhibition regions (mm) diameter against isolated strains *via* well diffusion method (Table S1). The inhibition areas found for all samples were 0.35–3.15 mm and 0.40–5.45 mm against *E. coli* and *S. aureus*, seaprately. The MgO/CNC-g-PAA (pH = 12.0) exhibited maximum inhibition area of 3.15 and 5.45 mm at maximal concentration (1000 μg/50 μL) while, null inhibition region observed at minimum (500 μg/50 μL) concentration. The bactericidal efficacy of all samples against G + ve was significantly high compared to G –ve, owing to differences in bacterial outer-membrane structure. Bactericidal efficiency of nanocomposite can be attributed to various phenomena, like electrostatic interactions with OH^- and H_2O fascinated at surface, resulting in reactive oxygen species (ROS) production, as depicted in Fig. S8. DI water (0 mm) and ciprofloxacin (4.25 mm, 5.35 mm) were used as a negative and positive control (Table S1). Additionally, DPPH assay and photocatalytic behavior were employed to examine free radical scavenging activity of synthesized sample (Fig. S7, Fig. S6), as elaborated in supporting text.

In silico molecular docking analysis are widely documented for evaluating possible mechanisms underlying diverse biological actions. Herein, docking analysis predicted MgO/CNC-g-PAA significantly blocked active site of DHFR and DNA gyrase B enzymes by strong binding interaction, which could inhibit the growth of *E. coli*. The best-docked conformation of DHFR enzyme displayed H-bonding interactions with Thr123, Ile14, Ile5, Ile94, Tyr100, Ala7, and Arg98 through a binding score of 5.70, as shown in Fig. 4(a-c) while binding score for a best-docked complex of MgO/CNC-g-PAA with DNA $gyrase_{E.\ coli}$ was 5.54 and formed a hydrogen bond with key amino acid residues Gly77, Thr165, Glu50, Val43, and Asn46, shown in Fig. 4(d-f).

Additionally, MgO/CNC-g-PAA interaction patterns were evaluated against DHFR and Tyrosyl-tRNA synthetase from *S. aureus*. Binding score of 8.60 were found in well-docked conformations of the selected compound into a DHFR active pocket. Thr46, Gln95, Ile14, Trp22, Ala7, and Asp27 interacted with MgO/CNC-g-PAA (Fig. 4 (j-l)). In tyrosyl-tRNA synthetase, following residues showed H-bonding with synthesized hydrogels; Gln190, Tyr36, Asp40, Tyr170, and Arg88 with highest binding score of 8.73, as depicted in Fig. 4 (g-i). Docking scores of each ligand-receptor complex, including the engaged key residues in binding interaction, is listed in Table S2. So, a substantial binding score and interaction indicated that MgO/CNC-g-PAA might be a potential

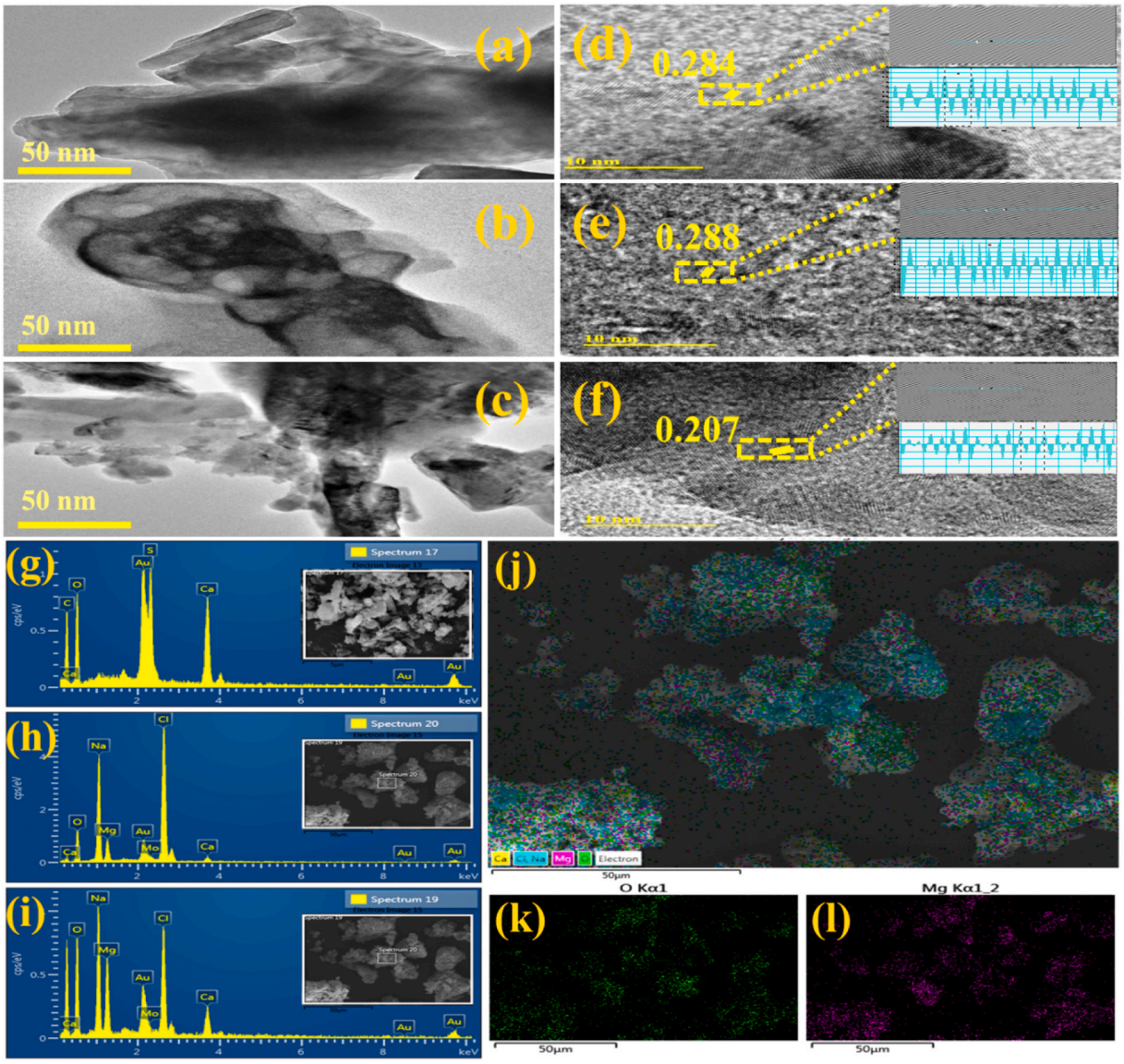

Fig. 3. (a-c) TEM and (d-f) d-spacing of synthesized nanocomposites; (a, d) CNC, (b, e) CNC-g-PAA, and (c, f) MgO/CNC-g-PAA (pH = 12.0), (g-i) EDS analysis of CNC, CNC-g-PAA, MgO/CNC-g-PAA, (j-l) Elemental mapping of (j) MgO/CNC-g-PAA (pH = 12.0), (k) O, and (l) Mg.

inhibitor of selected proteins.

3.4. DOX loading and pH-triggered based releasing efficiency

DOX was entrapped in synthesized nanocomposite hydrogels (CNC-g-PAA and MgO/CNC-g-PAA) (Fig. 5) by electrostatic interaction between positive and negative charges of DOX and –COOH-based nanocomposite hydrogels, respectively, and DOX loading results are described with detail in supporting text.

The pH-triggered based release of DOX from DOX-loaded hydrogels was evaluated using PBS with two different conditions (pH ~7.4 and 5.8) [11], which were chosen correspondingly to provide slightly alkaline and mild acidic environment for healthy and intra-tumoral cells (endosomes). Consequently, release rate of DOX was significantly lower at pH 7.4 compared to pH 5.8, as seen in Fig. 5. Regarding the DOX release efficiency, MgO/CNC-g-PAA (pH = 12.0) exhibited enhanced release rate than MgO/CNC-g-PAA (pH = 7.0) and CNC-g-PAA. Under neutral to slightly alkaline conditions (pH 7.4), DOX loaded MgO/CNC-g-PAA (pH = 12.0) hydrogel released drug <25 % after 24 h (Fig. 5d). In contrast, the system revealed a relatively rapid drug release rate in mild acidic environment (pH 5.8) as shown in Fig. 5(e, f). The observed rate of released DOX after first hour found 11.60 %, and after 24 h, released drug amount reached up to 53.7 %, ~2.2-fold higher than release rate at pH 7.4. The rapid release of DOX from nanocomposite hydrogels under mildly acidic conditions is related to enhancement of drug's hydrophilicity by boosting protonated amine groups and decreasing its electrostatic interaction. However, at pH 7.4, a significant electrostatic interaction between positively charged DOX molecules and negatively charged -COOH would inhibit DOX release from hydrogel. Therefore, nanocomposite hydrogels might be stable carriers for targeted drug administration with low leakage during blood circulation (pH 7.4); nevertheless, a considerable quantity of drug releases at the moderate acidic pH, as in intratumoral cells of lysosomes (pH 4–5) and endosomes (pH 5–6).

3.5. In vitro Cytotoxicity analyses

The MTT assay was conducted at breast cancer cells (MDA-MB-231) to evaluate *in-vitro* biocompatibility and anti-tumour potential of free DOX, DOX loaded CNC-g-PAA and DOX loaded MgO/CNC-g-PAA (pH =

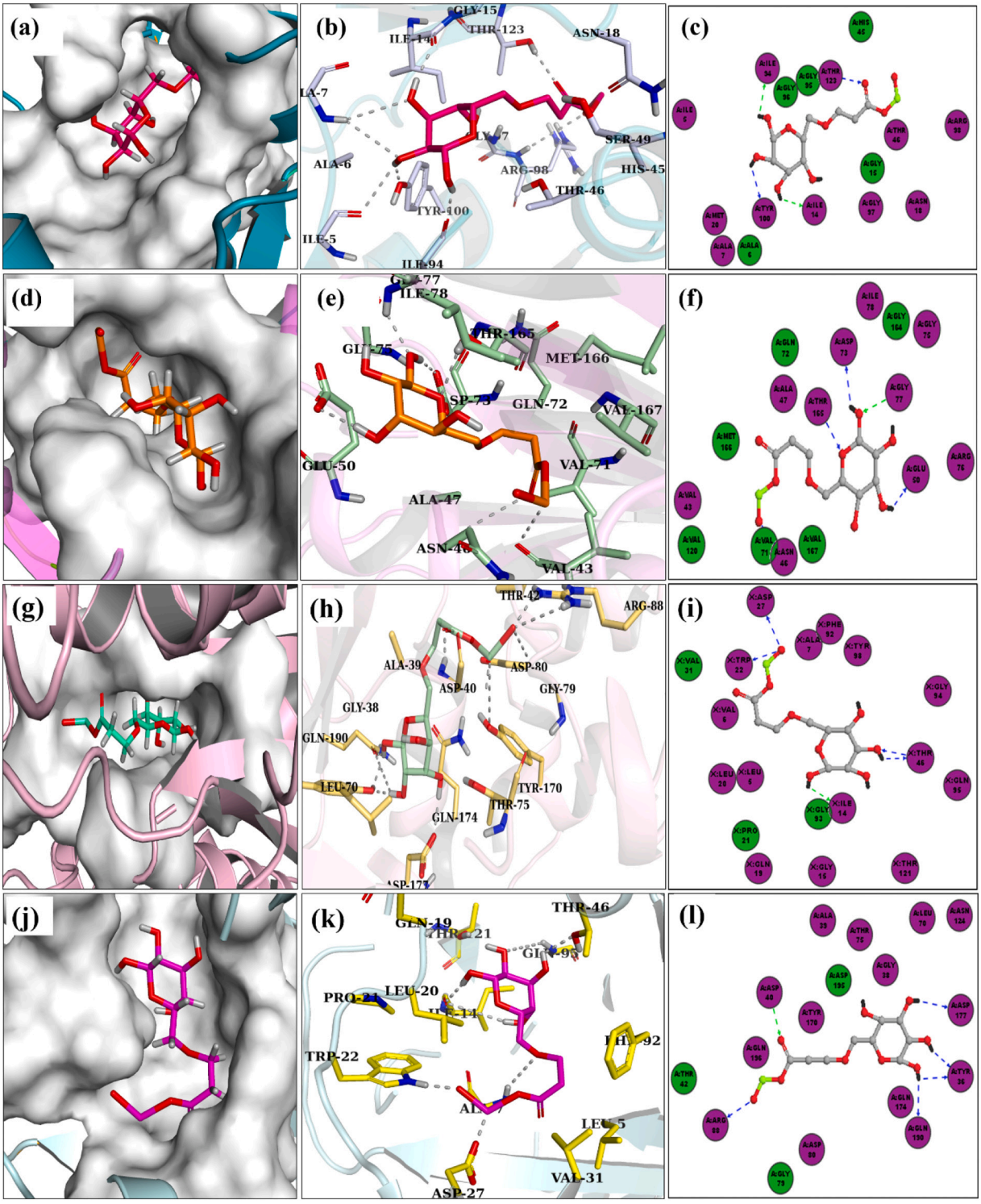

Fig. 4. Binding interaction pattern of the ligand (MgO/CNC-g-PAA) within the binding region of Dihydrofolate reductase (teal) shown in panels (a-c) and DNA gyrase B (violet) in panels (d-f) from *E. coli*. A docked ligand in the binding domain of both proteins is represented in panels (a, d), binding interaction pattern (b, e), and 2D view (c, f). Obtained ligand (MgO/CNC-g-PAA) binding modes in Tyrosyl-tRNA synthetase (light pink) binding domain in panels (g-i) and DHFR (light green) shown in panels (j-l) from *S. aureus*. A docked ligand in the binding domain of both proteins is represented in panels (g, j), binding interaction pattern (*h*, *k*), and 2D view (i, l). (For interpretation of the references to colour in this figure legend, the reader is referred to the web version of this article.)

12.0). The dose-dependent response of cell cytotoxicity assessed using various concentrations (3.9–500 μg/mL) of samples is shown in Fig. 6. The cytotoxic influence of drug-loaded nanocomposites (Fig. 6b) is significantly higher in contrast to drug-free nanocomposites (Fig. 6a), suggesting interference of nanocarriers by decreasing cancer cells viability as well as increasing drug update through endocytic process. These findings suggest MgO/CNC-g-PAA (pH = 12.0) synergistically enhanced DOX therapeutic efficacy by binding with DNA through intercalation and triggering a cascade of biochemical reactions resulting apoptotic cell death. Post-treatment 24 h, samples cell viability at

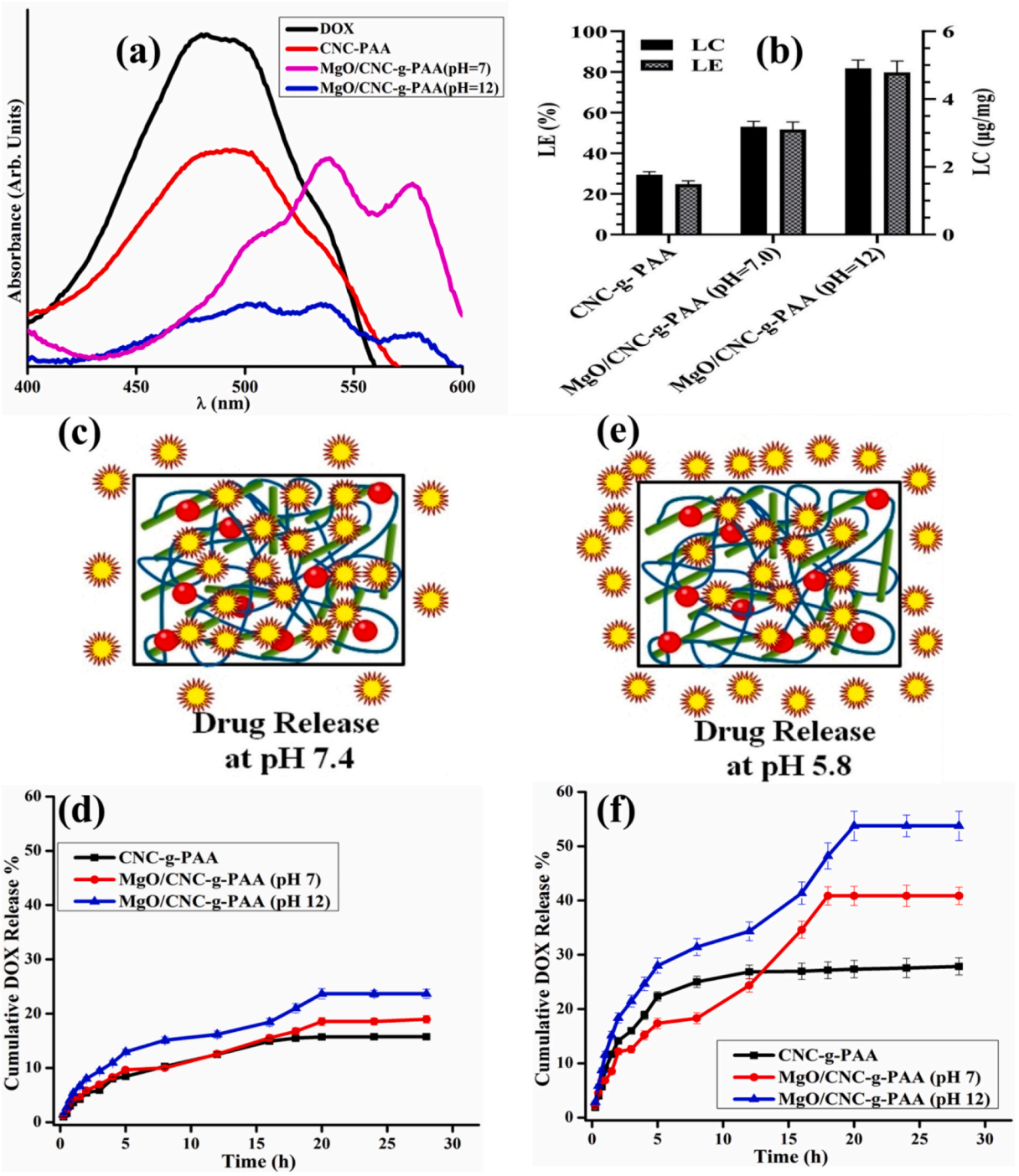

Fig. 5. (a) UV–vis spectra based drug loading profile of DOX into nanocomposites, (b) comparison of LC and LE of loaded drug. Schematic illustration of pH-triggered based DOX releasing from nanocomposites at (c) pH 7.4 and (e) 5.8. DOX release behavior from drug loaded samples (CNC-g-PAA, MgO/CNC-g-PAA (pH = 7.0), MgO/CNC-g-PAA (pH = 12.0)) at (d) pH 7.4 and (f) pH 5.8. Shown values are means ± standard deviation (n = 3).

numerous drug concentrations revealed substantially dose-dependent pattern. CNC-g-PAA acted as agonist with DOX to achieve synergetic effect against MDA-MB-231 cancer cells. The simultaneous release of DOX and CNC-g-PAA following internalisation into breast cancer cells and improved accumulation at tumour site could be reason for improved cytotoxicity [64]. The therapeutic efficacy of DOX and MgO/CNC-g-PAA formulation resulted substantial synergistic effect in contrast with CNC-g-PAA hydrogel, revealed through findings of *in vitro* cytotoxicity studies [23].

4. Conclusion

A novel metal-doped hydrogel (MgO/CNC-g-PAA) was successfully fabricated and evaluated for efficient antibacterial activity and targeted drug delivery. Morphological analyses revealed that generated CNC-g-PAA showed a porous sponge-like structure. Prepared nanocomposites revealed significant bactericidal efficiency against gram-positive bacteria. *In silico* analyses were performed to examine the mechanism behind bactericidal activity by binding interaction of nanocomposites with targeted proteins, and results revealed a good agreement with *in*

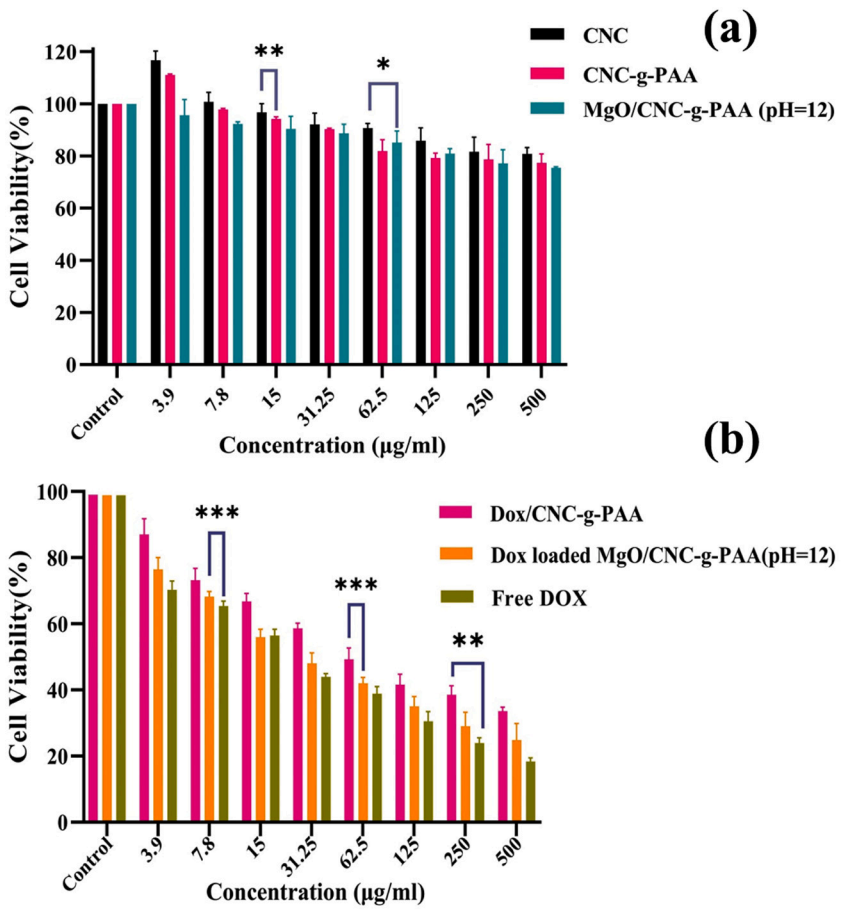

Fig. 6. (a) Cell viability of cells after treatment with different doses of drug-free nanocomposites, and (b) Cell viability of MDA-MB-231cells after exposure to different doses of drug-loaded hydrogel, DOX/CNC-g-PAA, DOX/MgO/CNC-g-PAA (pH = 12.0), and free DOX as a control sample. Shown values are means ± standard deviation ($n = 3$). One-way ANOVA was used for comparison between the groups, $^{*}p < 0.05$, $^{**}p < 0.007$, $^{***}p < 0.0005$.

vitro bactericidal activity. Moreover, these negatively charged hydrogels effectively entrapped the hydrophilic drug DOX by electrostatic interactions with LE of up to 79 %. *In vitro* release behavior of drug from DOX-loaded nanocomposite hydrogels revealed an efficient, stable, and controlled drug release at acidic pH 5.8. Because carboxyl groups protonate under acidic circumstances, so dropping the pH from 7.4 to 5.8, greatly increases the releasing rate of DOX. Finally, *in vitro* cytotoxicity study demonstrated that synergistic effect of DOX and MgO/CNC-g-PAA might trigger apoptosis in breast cancer cells (MDA-MB-231). Based on these findings, MgO/CNC-g-PAA hydrogels are potential candidates for targeted and controlled hydrophilic drug delivery.

CRediT authorship contribution statement

Iram Shahzadi: Conceptualization, Characterization, Formal analysis, writing-original draft. **Muhammad Islam:** Supervision, Review & editing, funding acquisition. **Hamid Saeed:** Characterization, Writing-review & editing. **Ali Haider:** Validation, Characterization, Writing-review & editing. **Anum Shahzadi:** Formal analysis Characterization, writing. **Junaid Haider:** Investigation, Writing, review & editing. **Nadeem Ahmed:** Characterization. **Muhammad Ikram:** Conceptualization, Funding acquisition, supervision, Project administration. **Anwar Ul-Hamid:** Characterization, Resources, Writing-review & editing. **Walid Nabgan:** Review & editing. **Hassaan AnwerRathore:** Supervision, Review & editing.

Declaration of competing interest

The authors declare no conflict of interest.

Acknowledgements

Authors are thankful to Higher Education Commission (HEC) Pakistan, through NRPU-20-17615 (Muhammad Ikram).

Appendix A. Supplementary data

Supplementary data to this article can be found online at https://doi.org/10.1016/j.ijbiomac.2022.08.142.

References

[1] J. Pan, K. Rostamizadeh, N. Filipczak, V. Torchilin, Polymeric co-delivery systems in cancer treatment: an overview on component drugs' dosage ratio effect, Molecules 24 (2019) 1035, https://doi.org/10.3390/molecules24061035.
[2] S. Senapati, A.K. Mahanta, S. Kumar, P. Maiti, Controlled drug delivery vehicles for cancer treatment and their performance, Signal Transduct. Target. Ther. 3 (2018) 7, https://doi.org/10.1038/s41392-017-0004-3.
[3] P. Arunkumar, S. Indulekha, S. Vijayalakshmi, R. Srivastava, In vitro comparative studies of zein nanoparticles and composite chitosan thermogels based injectable formulation of doxorubicin, J. Drug Deliv. Sci. Technol. 40 (2017) 116–124, https://doi.org/10.1016/J.JDDST.2017.05.015.
[4] K. Cho, X. Wang, S. Nie, Z.(Georgia) Chen, D.M. Shin, Therapeutic nanoparticles for drug delivery in cancer, Clin. Cancer Res. 14 (2008) 1310–1316, https://doi.org/10.1158/1078-0432.CCR-07-1441.
[5] K. Deepa, S. Singha, T. Panda, Doxorubicin nanoconjugates, J. Nanosci. Nanotechnol. 14 (2014) 892–904, https://doi.org/10.1166/jnn.2014.8765.

[6] M. Mohammadi, L. Arabi, M. Alibolandi, Doxorubicin-loaded composite nanogels for cancer treatment, J. Control. Release 328 (2020) 171–191, https://doi.org/10.1016/j.jconrel.2020.08.033.
[7] P. Couvreur, Nanoparticles in drug delivery: past, present and future, Adv. Drug Deliv. Rev. 65 (2013) 21–23, https://doi.org/10.1016/j.addr.2012.04.010.
[8] M. Alexandre, P. Dubois, Polymer-layered silicate nanocomposites: preparation, properties and uses of a new class of materials, Mater. Sci. Eng. R. Rep. 28 (2000) 1–63, https://doi.org/10.1016/S0927-796X(00)00012-7.
[9] M.S. Shim, Y.J. Kwon, Stimuli-responsive polymers and nanomaterials for gene delivery and imaging applications, Adv. Drug Deliv. Rev. 64 (2012) 1046–1059, https://doi.org/10.1016/j.addr.2012.01.018.
[10] K.S. Soppimath, T.M. Aminabhavi, A.R. Kulkarni, W.E. Rudzinski, Biodegradable polymeric nanoparticles as drug delivery devices, J. Control. Release 70 (2001) 1–20, https://doi.org/10.1016/S0168-3659(00)00339-4.
[11] F. Abedi, S. Davaran, M. Hekmati, A. Akbarzadeh, B. Baradaran, S.V. Moghaddam, An improved method in fabrication of smart dual-responsive nanogels for controlled release of doxorubicin and curcumin in HT-29 colon cancer cells, J. Nanobiotechnol. 19 (2021) 18, https://doi.org/10.1186/s12951-020-00764-6.
[12] S.K. Nair, S. Basu, B. Sen, M.-H. Lin, A.N. Kumar, Y. Yuan, P.J. Cullen, D. Sarkar, Colloidal gels with tunable mechanomorphology regulate endothelial morphogenesis, Sci. Rep. 9 (2019) 1072, https://doi.org/10.1038/s41598-018-37788-w.
[13] M.I.H. Mondal, M.O. Haque, in: Cellulosic Hydrogels: A Greener Solution of Sustainability, Springer, Cham, 2019, pp. 3–35, https://doi.org/10.1007/978-3-319-77830-3_4.
[14] J.K. Oh, R. Drumright, D.J. Siegwart, K. Matyjaszewski, The development of microgels/nanogels for drug delivery applications, Prog. Polym. Sci. 33 (2008) 448–477, https://doi.org/10.1016/j.progpolymsci.2008.01.002.
[15] D.E. Ciolacu, R. Nicu, F. Ciolacu, Cellulose-based hydrogels as sustained drug-delivery systems, Mater. (Basel, Switzerland) 13 (2020) 1–37, https://doi.org/10.3390/MA13225270.
[16] R. Rakhshaei, H. Namazi, H. Hamishehkar, M. Rahimi, Graphene quantum dot cross-linked carboxymethyl cellulose nanocomposite hydrogel for pH-sensitive oral anticancer drug delivery with potential bioimaging properties, Int. J. Biol. Macromol. 150 (2020) 1121–1129, https://doi.org/10.1016/j.ijbiomac.2019.10.118.
[17] T.R. Hoare, D.S. Kohane, Hydrogels in drug delivery: progress and challenges, Polymer (Guildf) 49 (2008) 1993–2007, https://doi.org/10.1016/J.POLYMER.2008.01.027.
[18] S. Behzadi Nia, M. Pooresmaeil, H. Namazi, Carboxymethylcellulose/layered double hydroxides bio-nanocomposite hydrogel: a controlled amoxicillin nanocarrier for colonic bacterial infections treatment, Int. J. Biol. Macromol. 155 (2020) 1401–1409, https://doi.org/10.1016/j.ijbiomac.2019.11.115.
[19] N. Kayra, A.Ö. Aytekin, in: Synthesis of Cellulose-Based Hydrogels: Preparation, Formation, Mixture, and Modification, 2018, pp. 1–28, https://doi.org/10.1007/978-3-319-76573-0_16-1.
[20] H. Du, W. Liu, M. Zhang, C. Si, X. Zhang, B. Li, Cellulose nanocrystals and cellulose nanofibrils based hydrogels for biomedical applications, Carbohydr. Polym. 209 (2019) 130–144, https://doi.org/10.1016/j.carbpol.2019.01.020.
[21] N. Halib, F. Perrone, M. Cemazar, B. Dapas, R. Farra, M. Abrami, G. Chiarappa, G. Forte, F. Zanconati, G. Pozzato, L. Murena, N. Fiotti, R. Lapasin, L. Cansolino, G. Grassi, M. Grassi, Potential applications of nanocellulose-containing materials in the biomedical field, Materials (Basel) 10 (2017) 977, https://doi.org/10.3390/ma10080977.
[22] M. Rizwan, R. Yahya, A. Hassan, M. Yar, A. Azzahari, V. Selvanathan, F. Sonsudin, C. Abouloula, pH sensitive hydrogels in drug delivery: brief history, properties, swelling, and release mechanism, material selection and applications, Polymers (Basel) 9 (2017) 137, https://doi.org/10.3390/polym9040137.
[23] M.R. Vakili, W. Mohammed-Saeid, A. Aljasser, J. Hopwood-Raja, B. Ahvazi, Y. Hrynets, M. Betti, A. Lavasanifar, Development of mucoadhesive hydrogels based on polyacrylic acid grafted cellulose nanocrystals for local cisplatin delivery, Carbohydr. Polym. 255 (2021), 117332, https://doi.org/10.1016/j.carbpol.2020.117332.
[24] P. Lu, Y. Lo Hsieh, Cellulose nanocrystal-filled poly(acrylic acid) nanocomposite fibrous membranes, Nanotechnology 20 (2009), https://doi.org/10.1088/0957-4484/20/41/415604.
[25] X. Hu, W. Wei, X. Qi, H. Yu, L. Feng, J. Li, S. Wang, J. Zhang, W. Dong, Preparation and characterization of a novel pH-sensitive salecan-g-poly(acrylic acid) hydrogel for controlled release of doxorubicin, J. Mater. Chem. B 3 (2015) 2685–2697, https://doi.org/10.1039/C5TB00264H.
[26] P. Thoniyot, M.J. Tan, A.A. Karim, D.J. Young, X.J. Loh, Nanoparticle-hydrogel composites: concept, design, and applications of these promising, multi-functional materials, Adv. Sci. 2 (2015), 1400010, https://doi.org/10.1002/ADVS.201400010.
[27] D. Pasqui, A. Atrei, G. Giani, M. De Cagna, R. Barbucci, Metal oxide nanoparticles as cross-linkers in polymeric hybrid hydrogels, Mater. Lett. 65 (2011) 392–395, https://doi.org/10.1016/J.MATLET.2010.10.053.
[28] P. Schexnailder, G. Schmidt, Nanocomposite polymer hydrogels, Colloid Polym. Sci. 287 (2009) 1–11, https://doi.org/10.1007/s00396-008-1949-0.
[29] A. Maleki, J. He, S. Bochani, V. Nosrati, M.-A. Shahbazi, B. Guo, Multifunctional photoactive hydrogels for wound healing acceleration, ACS Nano 15 (2021) 18895–18930, https://doi.org/10.1021/acsnano.1c08334.
[30] M. Safaei, M. Taran, M.M. Imani, H. Moradpoor, F. Rezaei, L. Jamshidy, R. Rezaei, Application of Taguchi method in the optimization of synthesis of cellulose-MgO bionanocomposite as antibacterial agent, Pol. J. Chem. Technol. 21 (2019) 116–122, https://doi.org/10.2478/pjct-2019-0047.
[31] L. Cai, J. Chen, Z. Liu, H. Wang, H. Yang, W. Ding, Magnesium oxide nanoparticles: effective agricultural antibacterial agent against ralstonia solanacearum, Front. Microbiol. 9 (2018) 790, https://doi.org/10.3389/FMICB.2018.00790/BIBTEX.
[32] S. Shen, P.S. Chow, F. Chen, R.B.H. Tan, Submicron particles of SBA-15 modified with MgO as carriers for controlled drug delivery, Chem. Pharm. Bull. 55 (2007) 985–991, https://doi.org/10.1248/cpb.55.985.
[33] S.V. Sudakaran, J.R. Venugopal, G.P. Vijayakumar, S. Abisegapriyan, A.N. Grace, S. Ramakrishna, Sequel of MgO nanoparticles in PLACL nanofibers for anti-cancer therapy in synergy with curcumin/β-cyclodextrin, Mater. Sci. Eng. C. 71 (2017) 620–628, https://doi.org/10.1016/j.msec.2016.10.050.
[34] Y.H. Leung, A.M.C. Ng, X. Xu, Z. Shen, L.A. Gethings, M.T. Wong, C.M.N. Chan, M. Y. Guo, Y.H. Ng, A.B. Djurišić, P.K.H. Lee, W.K. Chan, L.H. Yu, D.L. Phillips, A.P. Y. Ma, F.C.C. Leung, Mechanisms of antibacterial activity of MgO: non-ROS mediated toxicity of MgO nanoparticles towards Escherichia coli, Small 10 (2014) 1171–1183, https://doi.org/10.1002/smll.201302434.
[35] S. Makhluf, R. Dror, Y. Nitzan, Y. Abramovich, R. Jelinek, A. Gedanken, Microwave-assisted synthesis of nanocrystalline MgO and its use as a bacteriocide, Adv. Funct. Mater. 15 (2005) 1708–1715, https://doi.org/10.1002/adfm.200500029.
[36] P.-C. Maness, S. Smolinski, D.M. Blake, Z. Huang, E.J. Wolfrum, W.A. Jacoby, Bactericidal activity of photocatalytic TiO 2 reaction: toward an understanding of its killing mechanism, Appl. Environ. Microbiol. 65 (1999) 4094–4098, https://doi.org/10.1128/AEM.65.9.4094-4098.1999.
[37] H.A. Foster, I.B. Ditta, S. Varghese, A. Steele, Photocatalytic disinfection using titanium dioxide: spectrum and mechanism of antimicrobial activity, Appl. Microbiol. Biotechnol. 90 (2011) 1847–1868, https://doi.org/10.1007/s00253-011-3213-7.
[38] M. Ikram, A. Mahmood, A. Haider, S. Naz, A. Ul-Hamid, W. Nabgan, I. Shahzadi, J. Haider, I. Ahmad, S. Ali, Dye degradation, antibacterial and in-silico analysis of Mg/cellulose-doped ZnO nanoparticles, Int. J. Biol. Macromol. 185 (2021) 153–164, https://doi.org/10.1016/j.ijbiomac.2021.06.101.
[39] M. Ikram, T. Inayat, A. Haider, A. Ul-Hamid, J. Haider, W. Nabgan, A. Saeed, A. Shahbaz, S. Hayat, K. Ul-Ain, A.R. Butt, Graphene oxide-doped MgO nanostructures for highly efficient dye degradation and bactericidal action, Nanoscale Res. Lett. 16 (2021) 56, https://doi.org/10.1186/s11671-021-03516-z.
[40] M. Ikram, S. Aslam, A. Haider, S. Naz, A. Ul-Hamid, A. Shahzadi, M. Ikram, J. Haider, S.O.A. Ahmad, A.R. Butt, Doping of mg on ZnO nanorods demonstrated improved photocatalytic degradation and antimicrobial potential with molecular docking analysis, Nanoscale Res. Lett. 16 (2021) 78, https://doi.org/10.1186/s11671-021-03537-8.
[41] W. Liu, Z. Wang, Y. Luo, N. Chen, Application of nanocomposites in cancer immunotherapy, Nano Life 07 (2017), 1750008, https://doi.org/10.1142/S1793984417500088.
[42] J. Wang, L. Sui, J. Huang, L. Miao, Y. Nie, K. Wang, Z. Yang, Q. Huang, X. Gong, Y. Nan, K. Ai, MoS2-based nanocomposites for cancer diagnosis and therapy, Bioact. Mater. 6 (2021) 4209–4242, https://doi.org/10.1016/j.bioactmat.2021.04.021.
[43] T. Li, Y. Yu, H. Shi, Y. Cao, X. Liu, Z. Hao, Y. Ren, G. Qin, Y. Huang, B. Wang, Magnesium in combinatorial with valproic acid suppressed the proliferation and migration of human bladder cancer cells, Front. Oncol. 10 (2020) 2733, https://doi.org/10.3389/fonc.2020.589112.
[44] J. Wan, S. Geng, H. Zhao, X. Peng, Q. Zhou, H. Li, M. He, Y. Zhao, X. Yang, H. Xu, Doxorubicin-induced co-assembling nanomedicines with temperature-sensitive acidic polymer and their in-situ -forming hydrogels for intratumoral administration, J. Control. Release 235 (2016) 328–336, https://doi.org/10.1016/j.jconrel.2016.06.009.
[45] E. Lizundia, U. Goikuria, J.L. Vilas, F. Cristofaro, G. Bruni, E. Fortunati, I. Armentano, L. Visai, L. Torre, Metal nanoparticles embedded in cellulose nanocrystal based films: material properties and post-use analysis, Biomacromolecules 19 (2018) 2618–2628, https://doi.org/10.1021/acs.biomac.8b00243.
[46] J. Nsor-Atindana, H. Douglas Goff, W. Liu, M. Chen, F. Zhong, The resilience of nanocrystalline cellulose viscosity to simulated digestive processes and its influence on glucose diffusion, Carbohydr. Polym. 200 (2018) 436–445, https://doi.org/10.1016/j.carbpol.2018.07.088.
[47] N. Iwata, T. Koike, K. Tokuhiro, R. Sato, S. Furumi, Colloidal photonic crystals of reusable hydrogel microparticles for sensor and laser applications, ACS Appl. Mater. Interfaces 13 (2021) 57893–57907, https://doi.org/10.1021/ACSAMI.1C16500.
[48] C. You, L. Ning, H. Wu, C. Huang, F. Wang, A biocompatible and pH-responsive nanohydrogel based on cellulose nanocrystal for enhanced toxic reactive oxygen species generation, Carbohydr. Polym. 258 (2021), 117685, https://doi.org/10.1016/j.carbpol.2021.117685.
[49] M. Ikram, A. Mahmood, A. Haider, S. Naz, A. Ul-Hamid, W. Nabgan, I. Shahzadi, J. Haider, I. Ahmad, S. Ali, Dye degradation, antibacterial and in-silico analysis of Mg/cellulose-doped ZnO nanoparticles, Int. J. Biol. Macromol. 185 (2021) 153–164, https://doi.org/10.1016/j.ijbiomac.2021.06.101.
[50] M. Ikram, S. Hayat, M. Imran, A. Haider, S. Naz, A. Ul-Hamid, I. Shahzadi, J. Haider, A. Shahzadi, W. Nabgan, S. Ali, Novel Ag/cellulose-doped CeO2 quantum dots for efficient dye degradation and bactericidal activity with molecular docking study, Carbohydr. Polym. 269 (2021), 118346, https://doi.org/10.1016/j.carbpol.2021.118346.
[51] K. Prusty, S.K. Swain, Release of ciprofloxacin drugs by nano gold embedded cellulose grafted polyacrylamide hybrid nanocomposite hydrogels, Int. J. Biol. Macromol. 126 (2019) 765–775, https://doi.org/10.1016/j.ijbiomac.2018.12.258.

[52] W.-M. Cheng, X.-M. Hu, Y.-Y. Zhao, M.-Y. Wu, Z.-X. Hu, X.-T. Yu, Preparation and swelling properties of poly(acrylic acid-co-acrylamide) composite hydrogels, E-Polymers 17 (2017) 95–106, https://doi.org/10.1515/epoly-2016-0250.
[53] S. Sarkar, C. Hazra, M. Chatti, V. Sudarsan, V. Mahalingam, Enhanced quantum efficiency for Dy3+ emissions in water dispersible PbF2 nanocrystals, RSC Adv. 2 (2012) 8269, https://doi.org/10.1039/c2ra21113k.
[54] K. Zhang, Y. Zhuang, J. Li, X. Liu, S. He, Poly(Acrylic Acid)-modified MoS2 nanoparticle-based transdermal delivery of atenolol, Int. J. Nanomedicine 15 (2020) 5517–5526, https://doi.org/10.2147/IJN.S257906.
[55] M. Pooresmaeil, H. Namazi, Facile coating of the methotrexate-layered double hydroxide nanohybrid via carboxymethyl starch as a pH-responsive biopolymer to improve its performance for colon-specific therapy, Eur. Polym. J. 165 (2022), 111026, https://doi.org/10.1016/j.eurpolymj.2022.111026.
[56] M.H. Zahir, M.M. Rahman, K. Irshad, M.M. Rahman, Shape-stabilized phase change materials for solar energy storage: MgO and Mg(OH)2 mixed with polyethylene glycol, Nanomaterials 9 (2019) 1773, https://doi.org/10.3390/nano9121773.
[57] A. M.V, M. Harb, R. Sundaram, Synthesis and characterization of cellulose/TiO2 nanocomposite: evaluation of in vitro antibacterial and in silico molecular docking studies, Carbohydr. Polym. 249 (2020), 116868, https://doi.org/10.1016/j.carbpol.2020.116868.
[58] J. Gong, J. Li, J. Xu, Z. Xiang, L. Mo, Research on cellulose nanocrystals produced from cellulose sources with various polymorphs, RSC Adv. 7 (2017) 33486–33493, https://doi.org/10.1039/C7RA06222B.
[59] L. Lim, N. Rosli, I. Ahmad, A.Mat Lazim, M.Mohd Amin, Synthesis and swelling behavior of pH-sensitive semi-IPN superabsorbent hydrogels based on poly(acrylic acid) reinforced with cellulose nanocrystals, Nanomaterials 7 (2017) 399, https://doi.org/10.3390/nano7110399.
[60] A. Pinkert, K.N. Marsh, S. Pang, M.P. Staiger, Ionic liquids and their interaction with cellulose, Chem. Rev. 109 (2009) 6712–6728, https://doi.org/10.1021/CR9001947/ASSET/CR9001947.FP.PNG_V03.
[61] Y. Wu, L. Wang, Y. Qing, N. Yan, C. Tian, Y. Huang, A green route to prepare fluorescent and absorbent nano-hybrid hydrogel for water detection, Sci. Rep. 7 (2017) 4380, https://doi.org/10.1038/s41598-017-04542-7.
[62] N. Karami, F. Davar, S. Hasani, Effect of annealing temperature and chelating agent concentration on the phase evolution, morphology and heavy metal removal efficiency of nanosized spinel, Mater. Res. Express. 6 (2019), https://doi.org/10.1088/2053-1591/AB3263.
[63] F. Henry, P. Marchal, J. Bouillard, A. Vignes, O. Dufaud, L. Perrin, The effect of agglomeration on the emission of particles from nanopowders flow, Chem. Eng. Trans. (2013) 811–816, https://doi.org/10.3303/CET1331136.
[64] Y. Zhang, C. Yang, W. Wang, J. Liu, Q. Liu, F. Huang, L. Chu, H. Gao, C. Li, D. Kong, Q. Liu, J. Liu, Co-delivery of doxorubicin and curcumin by pH-sensitive prodrug nanoparticle for combination therapy of cancer, Sci. Rep. 6 (2016) 21225, https://doi.org/10.1038/srep21225.